Materials Science and Engineering C 77 (2017) 84–91

Contents lists available at ScienceDirect

Materials Science and Engineering C

journal homepage: www.elsevier.com/locate/msec

The controlled drug release by pH-sensitive molecularly imprinted nanospheres for enhanced antibacterial activity

Congyang Mao [a], Xianzhou Xie [a], Xiangmei Liu [a], Zhenduo Cui [b], Xianjin Yang [b], K.W.K. Yeung [c], Haobo Pan [d], Paul K. Chu [e], Shuilin Wu [a,b,*]

[a] Hubei Collaborative Innovation Center for Advanced Organic Chemical Materials, Ministry-of-Education Key Laboratory for the Green Preparation and Application of Functional Materials, Hubei Key Laboratory of Polymer Materials, School of Materials Science & Engineering, Hubei University, Wuhan 430062, China
[b] School of Materials Science & Engineering, Tianjin University, Tianjin 300072, China
[c] Department of Orthopaedics & Traumatology, Li Ka Shing Faculty of Medicine, The University of Hong Kong, Pokfulam, Hong Kong, China
[d] Center for Human Tissues and Organs Degeneration, Shenzhen Institutes of Advanced Technology, Chinese Academy of Sciences, Shenzhen 518055, China
[e] Department of Physics & Materials Science, City University of Hong Kong, Tat Chee Avenue, Kowloon, Hong Kong, China

ARTICLE INFO

Article history:
Received 7 February 2017
Received in revised form 26 March 2017
Accepted 27 March 2017
Available online 29 March 2017

Keywords:
pH-sensitive
Molecularly imprinted nanospheres
Polymerization
Drug delivery
Antibacterial

ABSTRACT

In this study, we prepared pH-sensitive hybrid nanospheres through the implementation of a facile molecularly imprinted polymer (MIP) technique combined with a UV-initiated precipitation polymerization method using vancomycin (VA) for the templates. During the course of this investigation, both 2-hydroxyethyl methacrylate (HEMA) and 2-(diethylamino) ethyl methacrylate (DEAEMA) were utilized as the functional monomers, while ethylene glycol dimethacrylate (EGDMA) was used as a cross-linker. The obtained MIP nanospheres exhibited well-controlled particle size, with a drug loading capacity of about 17%, much higher than that of the non-imprinted polymer (NIP) nanospheres (5%). In addition, the VA loading quantity was closely correlated with the dosage of the cross-linking agent, and the MIP nanospheres exhibited a slower and more controlled VA release rate than the NIP nanospheres. Moreover, these MIP nanospheres were sensitive to pH values, and consequently showed an increasing release rate of VA as the pH level was decreased. The VA-loaded MIP nanospheres showed the higher antibacterial ratio of over 92% against *Staphylococcus aureus* (*S. aureus*) while the NIP nanospheres were friendly to *S. aureus*. These MIP nanospheres can be promising for targeting drug delivery system to achieve specific therapies such as preventing bacterial infections and killing cancer cells without damaging health cells and tissues.

1. Introduction

Currently, bacterial infections and their related complications often lead to the failure of implants [1], and the common method of rectification is to remove the implants and perform a secondary surgery, which generally brings unnecessary pain and additional costs for the patients [2,3]. In order to improve the success rate of implants and prevent these infections, building an active coating on the implant surface is considered to be an effective strategy, such as a coating capable of the controlled release of antibacterial drugs or agents on the implant surface [4–6]. It has been reported that the continuous local release of anti-inflammatory agents around the implants could help to control inflammation [5]. However, it is still a major challenge to control this release long-effectively.

In recent years, it has been reported that the stimuli-responsive molecularly imprinted polymer (MIP), a novel kind of functional material, can be synthesized by the copolymerization of the cross-linkers and the functional monomers in the presence of the template molecules due to its fascinating properties. The MIP can not only respond to external stimuli such as the pH levels [6,7], temperature changes [8,9], electric field interference [10,11], magnetic field interference [12–15], and photonic irradiation effects [8,16–18], among other factors, but it also possesses molecular recognition ability for template molecules [19,20]. More specifically, the pH-responsive MIP for drug delivery has attracted significant attention recently for its superior desired selectivity, which can result in a higher loading capacity and a more effectively controlled release of antibacterial drugs [21–23].

Vancomycin (VA), a clinically important first-generation glycopeptide antibiotic [24,25], has already been proven to exhibit sustained microbiologic inhibitory activity for implants due to the formation of a

* Corresponding author at: Hubei Collaborative Innovation Center for Advanced Organic Chemical Materials, Ministry-of-Education Key Laboratory for the Green Preparation and Application of Functional Materials, Hubei Key Laboratory of Polymer Materials, School of Materials Science & Engineering, Hubei University, Wuhan 430062, China.
E-mail addresses: shuilin.wu@hubu.edu.cn, sxwsl1976@163.com (S. Wu).

http://dx.doi.org/10.1016/j.msec.2017.03.259
0928-4931/

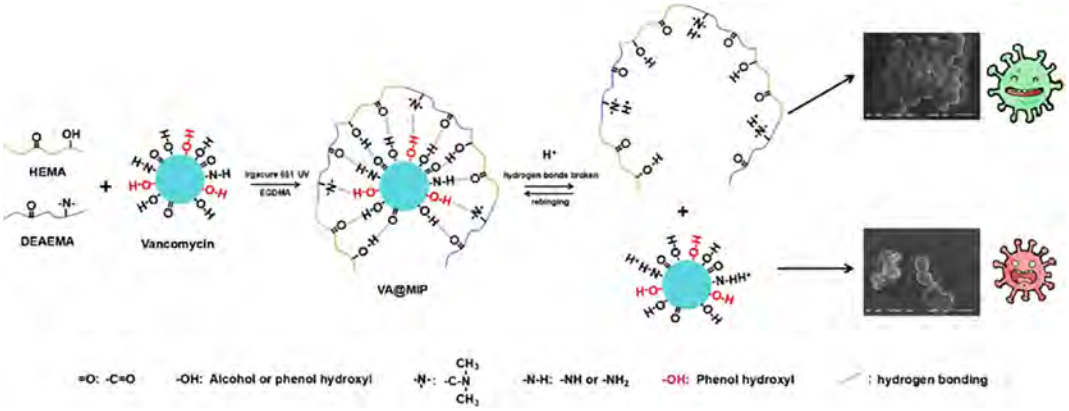

Scheme 1. Imprinting mechanism for the drug delivery system of VA@MIPs.

local release system, thus preventing postsurgical infections [26–28]. Therefore, the objective of the current study was to build an active surface system to enhance VA loading capacity, and to facilitate the sustained release of drugs for enhanced antibacterial activity. To achieve this goal, molecularly imprinted technology based on hydrogen bonding between the template molecule VA and functional monomers, i.e.,

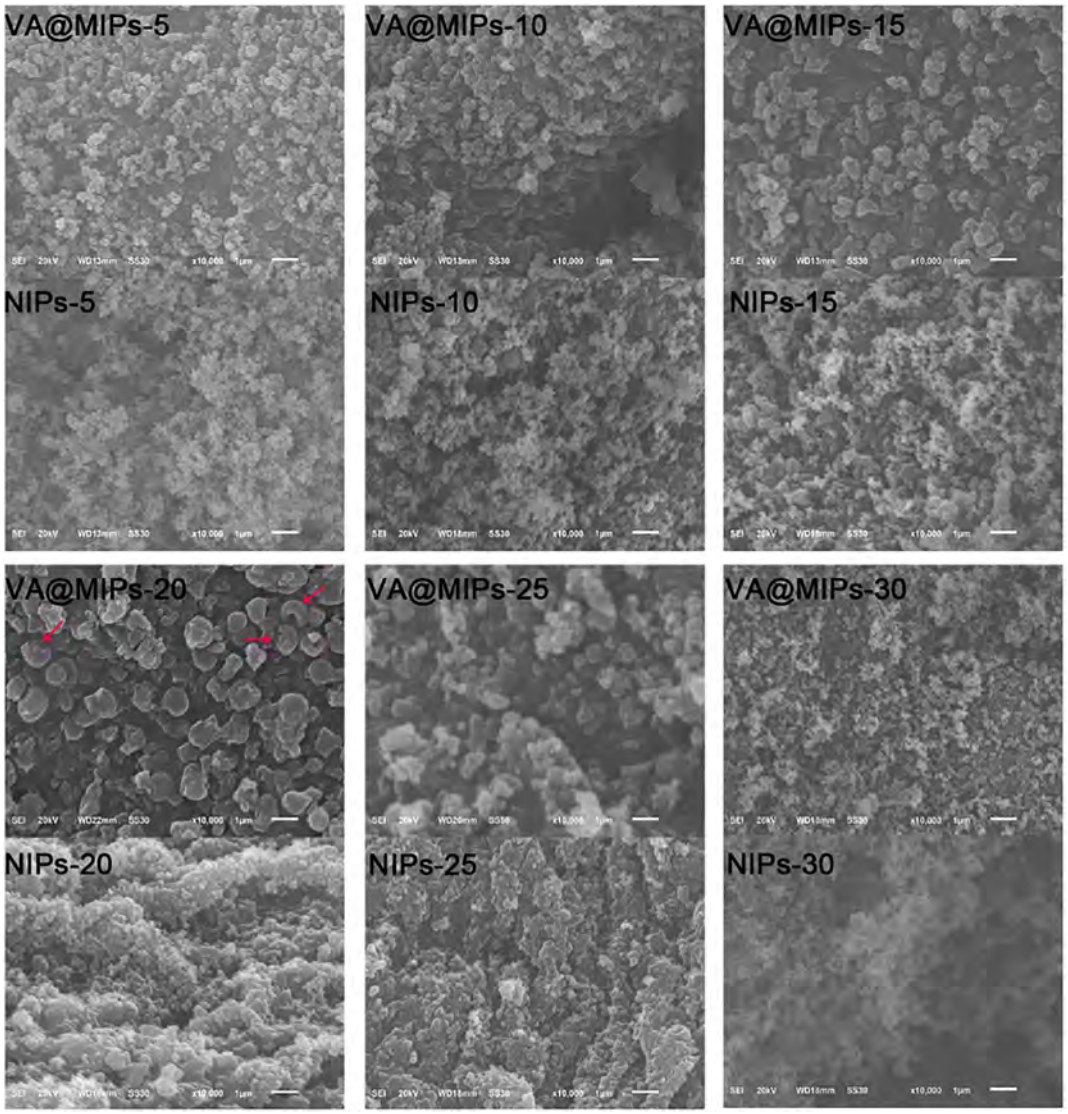

Fig. 1. SEM images of the VA@MIPs and NIPs prepared via UV-initiated precipitation polymerization with different dosage of cross-linker EGDMA.

HEMA and DEAEMA, was employed to prepare MIP nanospheres through a UV-initiated precipitation polymerization technique.

2. Experiment procedures

2.1. Materials

The vancomycin (VA) was purchased from Wuhan Dahua Pharmaceutical Co., Ltd., Wuhan, China. The 2-hydroxyethyl methacrylate (HEMA), 2-(diethylamino) ethyl methacrylate (DEAEMA), ethylene glycol dimethacrylate (EGDMA), and the photoinitiator Irgacure651 were purchased from Aladdin Shanghai Co., Ltd., Shanghai, China.

2.2. Fabrication of pH-sensitive VA-loaded MIP nanospheres and NIP nanospheres

The VA-loaded molecularly imprinted nanospheres (VA@MIPs) were prepared through the following procedures. The template VA (0.15 mmol), functional monomers HEMA (1 mmol), and DEAEMA (1 mmol) were dissolved separately in 10 mL deionized water. Then, these solutions were sequentially added into a two-neck round-bottom flask. The cross-linker EGDMA with different concentrations (5 mmol, 10 mmol, 15 mmol, 20 mmol, 25 mmol, and 30 mmol) and the photoinitiator Irgacure 651 (2 wt% of total monomers) were then dissolved in 30 mL ethanol. Afterward, the mixture was slowly dropped into the above two-neck round-bottom flask. Thereafter, the solution was purged with nitrogen gas for 15 min, and then subsequently sealed and irradiated by 12 W UV-light ($\lambda = 365$ nm) at room temperature for 1 h with stirring. The formed suspension was filtered and washed 5 times with de-ionized water in order to remove the residual functional monomers, the cross-linker, and the templates. Correspondingly, these final products were labeled as VA@MIPs-5, VA@MIPs-10, VA@MIPs-15, VA@MIPs-20, VA@MIPs-25, and VA@MIPs-30, respectively. The non-imprinted polymer nanospheres (NIPs) were prepared with the same method but without the presence of the template of VA, and were labeled as NIPs-5, NIPs-10, NIPs-15, NIPs-20, NIPs-25, and NIPs-30, respectively. All of the prepared samples were then freeze-dried for 12 h.

2.3. VA loading into the NIPs

VA was loaded into the NIPs through the use of the soaking method. Then, 20 mg of NIPs were immersed in 10 mL VA aqueous solution with a concentration of 500 μg/mL. After that, the mixture was ultrasonicated for 30 min, and then placed on a shaking table for 24 h at room temperature. Finally, the mixture was filtered and freeze-dried for 12 h. Correspondingly, these final products were labeled as VA@NIPs-5, VA@NIPs-10, VA@NIPs-15, VA@NIPs-20, VA@NIPs-25, and VA@NIPs-30, respectively. To calculate the VA loading content, 2 mL of filtrates were extracted and analyzed with a microplate reader (SpectraMax i3, Molecular Devices, U.S.A) at 280 nm.

2.4. Characterization of the VA@MIPs and NIPs

The morphologies of both the VA@MIPs and NIPs were observed through the use of scanning electron microscopy (SEM, JSM6510LV) and transmission electron microscope (TEM, Tecnai G20). In order to estimate the drug load, the VA@MIPs and NIPs were characterized with thermos-gravimetric analysis (TGA, Mettler-Toledo). The samples were heated from 30 °C to 800 °C at a heating rate of 20 °C/min in N_2 flow (30 mL/min), with N_2 as the balance gas (20 mL/min).

2.5. VA release tests

To determine the in vitro VA release profile, 20 mg of the VA-loaded nanospheres were placed into dialysis tubing and suspended in 5 mL phosphate-buffered saline (PBS) solution; they were then immersed in 95 mL PBS solution. After this step, all of the solutions were stored in a beaker and subsequently sealed at 37 °C. At certain time intervals, 1 mL of the solutions were extracted for VA quantity analysis by a microplate reader (SpectraMax i3, Molecular Devices) at 280 nm and then 1 mL fresh PBS was poured into the solutions.

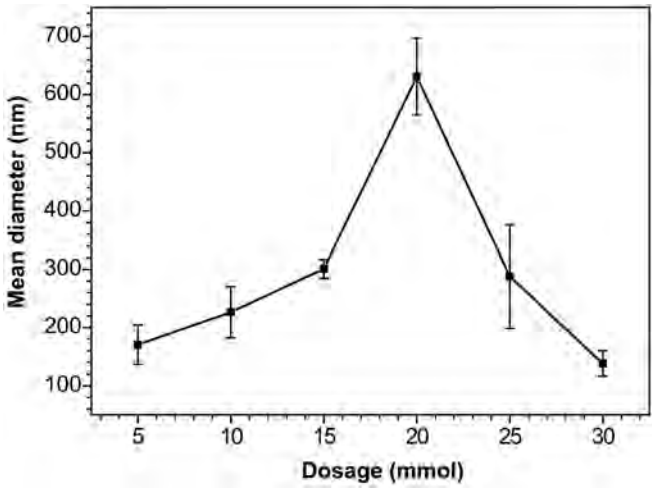

Fig. 2. The particle size distributions of the VA@MIPs prepared with different dosage of EGDMA.

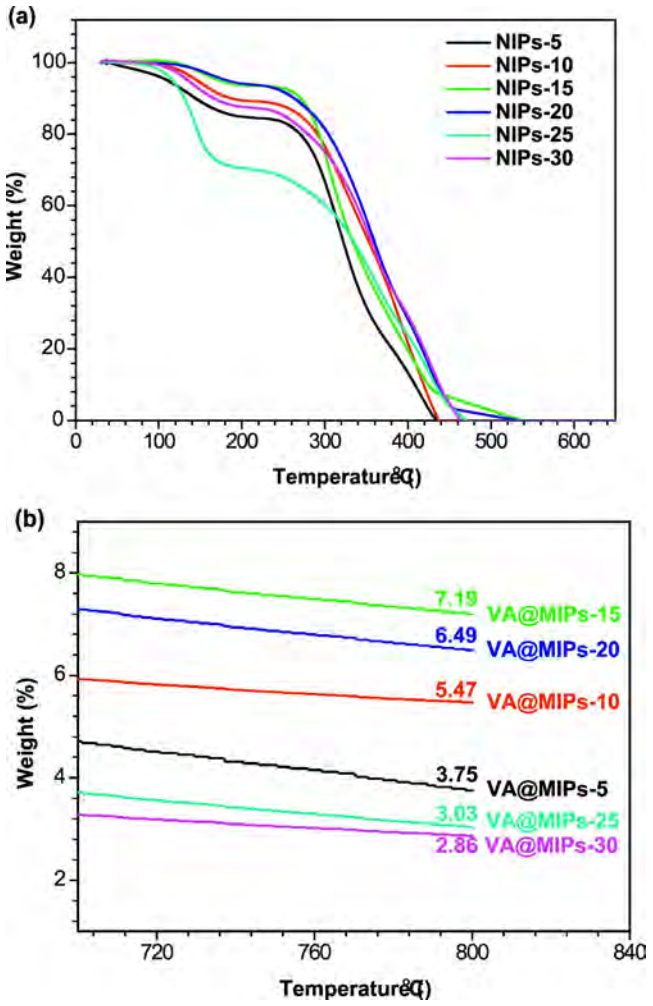

Fig. 3. TGA profiles of the (a) NIPs and (b) VA@MIPs prepared with different dosage of EGDMA.

To study the release behaviors of VA from the MIP nanospheres (MIPs) at different pH values, 20 mg of VA@MIPs-20 were placed in dialysis tubing and suspended in 5 mL PBS solution at different pH values of 5.2, 6.4, and 7.4. The procedures were the same as those mentioned above. All of the release experiments were performed three times, with three samples used each time.

2.6. Antibacterial activity assay

Antibacterial activity of the VA@MIPs and NIPs against *Staphylococcus aureus* (*S. aureus*) were studied using the quantitive measuring optical density (OD) at 600 nm by a microplate reader (SpectraMax i3, Molecular Devices). The concentration of *S. aureus* is about 1×10^7 CFU/mL. For the quantitive measurement of optical density, 2 mg of the samples and 1 mg of VA were placed into each well of a 48-well plate, respectively, and the blank plates were served as control. Then 600 μL of the bacterial suspension was added into each well with constant shaking at 37 °C in a shaker incubator for 24 h. The assay was performed in triplicates, with three replicates for each independent test. After that, 20 μL of the bacterial suspension was collected and spread on Luria-Bertani (LB) agar plate and incubated at 37 °C for 36 h to form viable colony units.

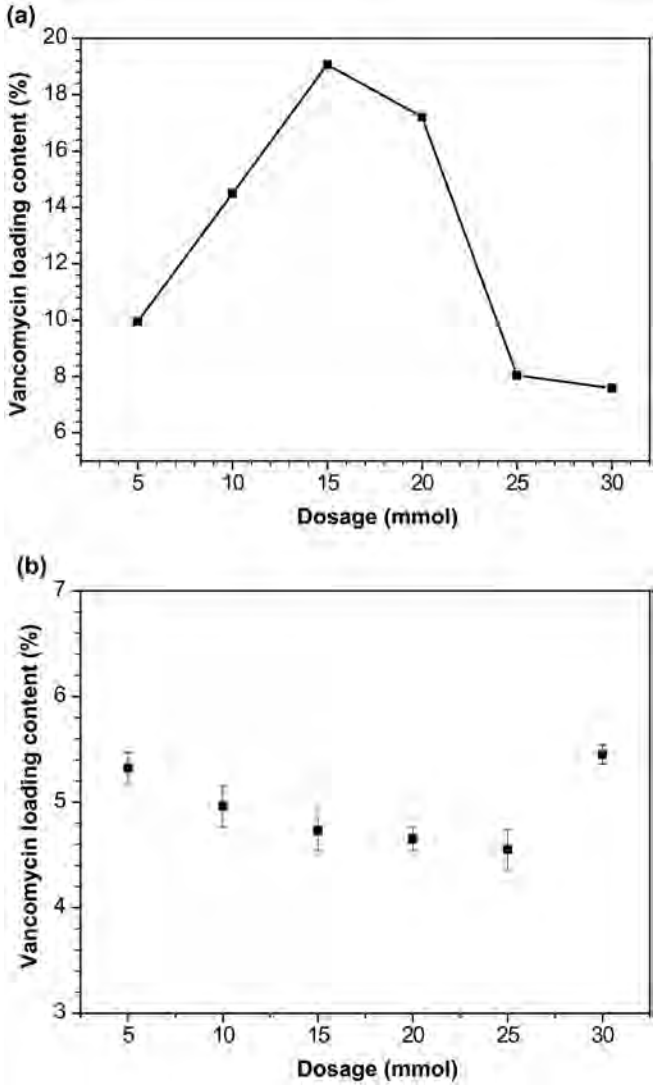

Fig. 4. VA loading contents of the (a) MIPs and (b) NIPs prepared with different dosage of EGDMA.

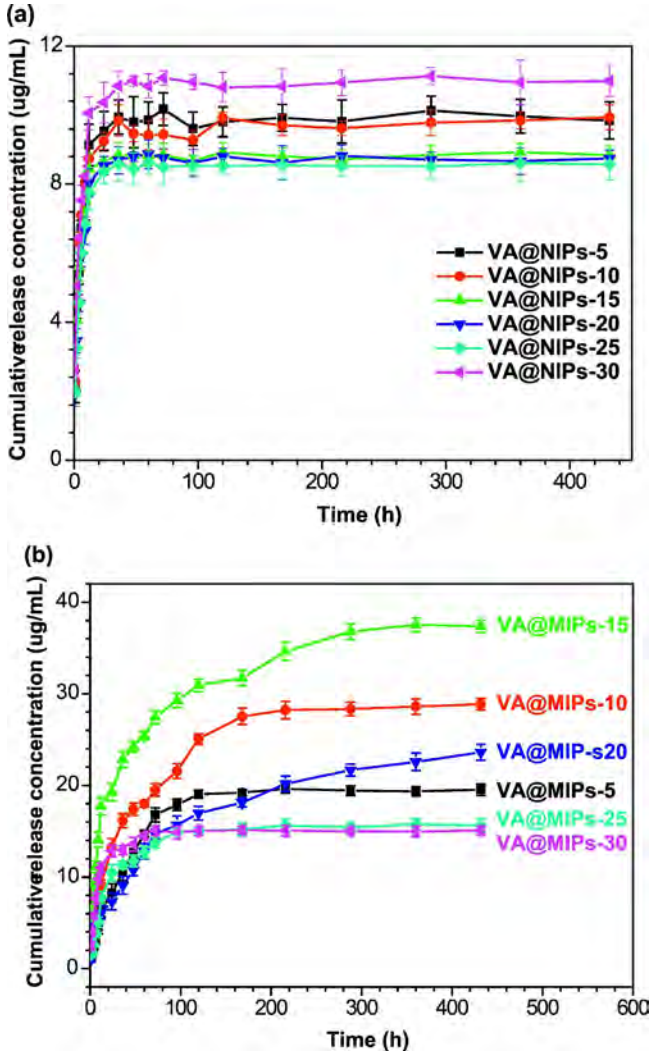

Fig. 5. In vitro VA release profiles of the (a) VA@NIPs and (b) VA@MIPs prepared with different dosage of EGDMA ($n = 3$) (pH = 7.4, PBS, 37 °C).

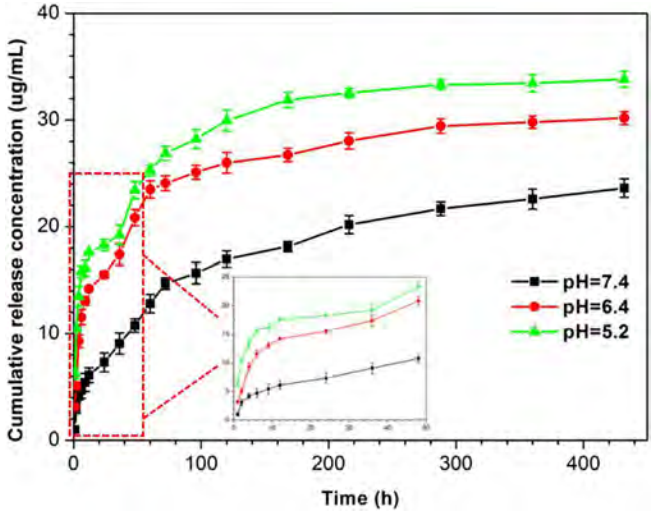

Fig. 6. In vitro VA release profiles of the VA@MIPs-20 at various pH PBS solutions at 37 °C ($n = 3$).

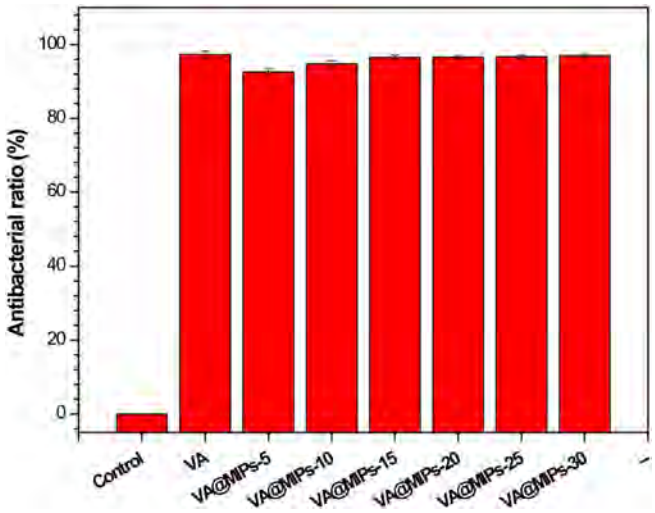

Fig. 7. Antibacterial activity of the VA@MIPs prepared with different dosage of EGDMA against *S. aureus* after 24 h incubation at 37 °C ($n = 3$).

For SEM observation, the samples were processed as the same with the quantitive measuring optical density. After the bacterial adhesion process, the bacterial suspension was drawn back completely. Then the adherent *S. aureus* on the bottom of the 48-well plate was fixed with 2.5% glutaraldehyde for 2 h, and then dehydrated by alcohol with different concentrations of 30%, 50%, 70%, 90% and 100% successively for 15 min and finally dried in air for SEM observation.

3. Results and discussion

3.1. Formation of the VA@MIPs and NIPs by UV-initiated precipitation polymerization

In the typical molecular imprinting process, reversible bonding between the polymerizable functional monomers and the templates usually includes reversible covalent bond(s), electrostatic interactions, coordination with a metal center, or hydrophobic or van der Waals interactions [22]. In this work, non-covalent bonds based on hydrogen bonding between the template molecule VA and the functional monomers HEMA and DEAEMA could be easily formed between the —OH and —C═O groups, the —OH and the —C—N groups, as well as the —NH (—NH_2) and the —C═O groups in the synthesizing process of VA@MIPs, as shown in Scheme 1. During the process, the precipitation polymerization method was adopted because this method was very simple to execute, and no surfactants or stabilizers were needed [29]. Moreover, monodispersed and highly-cross-linked nanospheres could be easily prepared. Generally, the precipitation polymerization is heat-initiated by 2,2′-azobisisbutyronitrile (AIBN), and the reaction is generally conducted at 70 °C [30], which could result in the thermal decomposition of the templates. In this experiment, the templates were

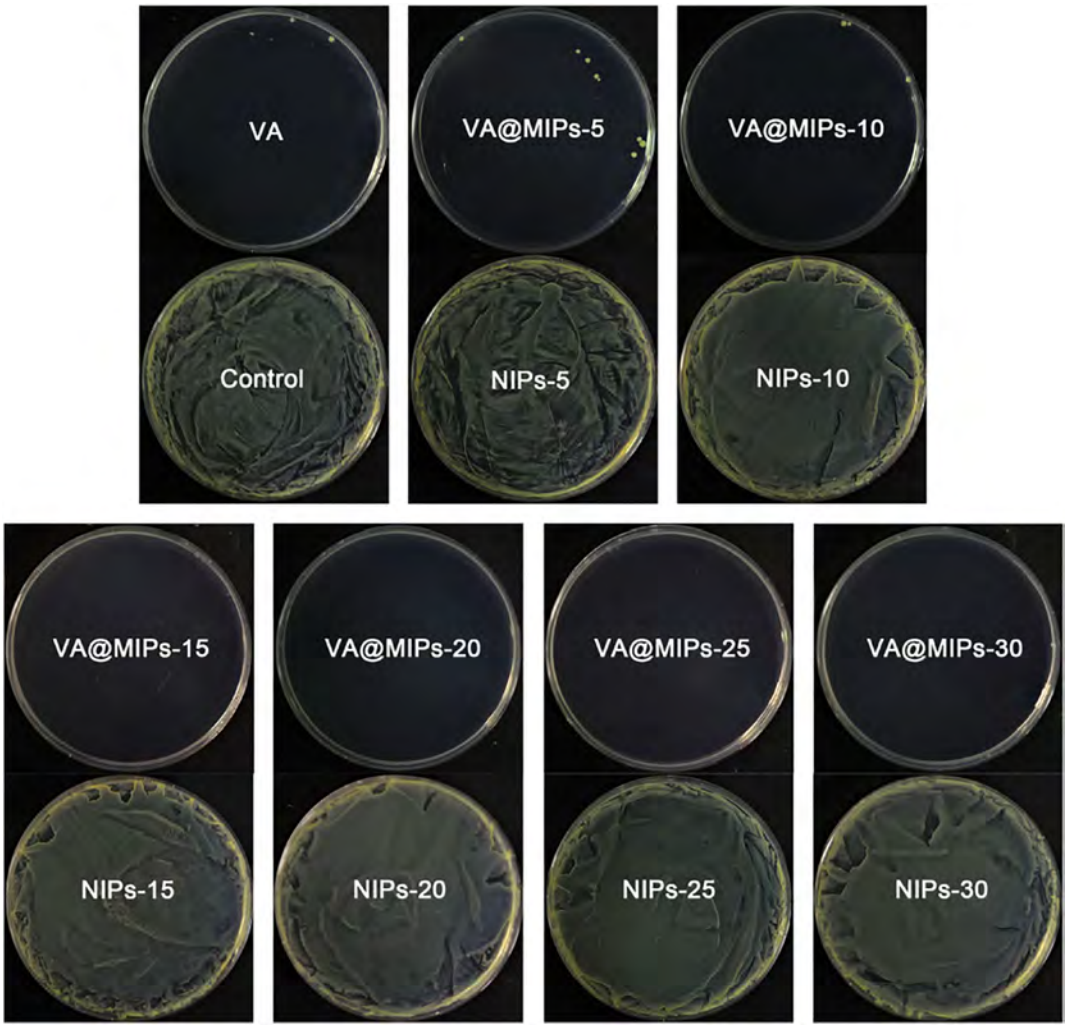

Fig. 8. Photographs of *S. aureus* colonies in Luria-Bertani (LB) media after co-cultured with the VA@MIPs and NIPs prepared with different dosage of EGDMA for 24 h at 37 °C.

temperature-sensitive, as shown in Fig. S1, and they were decomposed for 2.3% at 70 °C. Thus, UV-initiated polymerization was used instead of the heat initiation technique to avoid the high-reaction temperatures and thus to provide a high rate of polymerization.

3.2. Surface characterization of the VA@MIPs and NIPs

Fig. 1 shows the SEM images of the VA@MIPs and NIPs. One of the most significant differences between the VA@MIPs and NIPs was that the NIPs exhibited large aggregates as compared with the VA@MIPs. This may be attributed to the fact that the templates were able to influence the morphology of the resulting VA@MIPs [31], which can also be proven by TEM investigation. As shown in Fig. S2, the content of cross-linking agent exhibited great effect on the morphologies and size of VA@MIPs. In the case of VA@MIPs-5, it shows a cross-linked meshy structure. As the content of cross-linking agent increases, VA@MIPs exhibit independent nano particles, and the particle size is also increased. When the concentration of EGDMA reached to 20 mmol, the largest particle size could be obtained. The further increase of this agent could result in the decrease of particle size, and VA@MIPs-30 exhibited the similar netty structure to VA@MIPs-5. On the contrary, there is no obvious influence on NIPs. Regardless of the content of cross-linking agent, all NIPs exhibited great agglomeration. Fig. 2 displays the size evolution of the VA@MIPs with the different dosages of the cross-linking agent EGDMA. With the increase of the dosage of the cross-linking agent from 5 to 30 mmol, the particle size of the VA@MIPs showed a trend of an initial increase and a subsequent decrease, which could be attributed to the fact that the polymerization degree of the VA@MIPs increased with the increase of the dosage of the cross-linking agent, thus reaching the optimal level, while a higher dosage of the cross-linking agent resulted in excessive cross-linking. This explains why the VA@MIPs-20 displayed the largest diameter of about 650 nm among all of the groups.

3.3. VA loading capacity of the MIPs and NIPs

According to the TGA profiles, all of the NIPs were completely decomposed prior to 800 °C exposure (as shown in Fig. 3a), while the VA@MIPs still had residuals from 2.86 to 7.19% at 800 °C (as shown in Fig. 3b). The TGA results showed that pure VA could remain at rates of 37.7% at 800 °C (Fig. S1). Based on this assessment, the VA loading contents of the MIPs could be calculated according to following Eq. (1):

$$\text{Loading content} = \frac{W2^{*}100\%}{W1} \quad (1)$$

where W1 is 37.7%, the residual mass fraction of VA at 800 °C gained from the TGA profile of VA. W2 represents the residual mass fractions of the VA@MIPs at 800 °C (Fig. 3b), the residual mass fractions were 3.75%, 5.47%, 7.19%, 6.49%, 3.03%, and 2.86% for VA@MIPs-5, VA@MIPs-10, VA@MIPs-15, VA@MIPs-20, VA@MIPs-25, and VA@MIPs-30, respectively. Correspondingly, the VA loading contents were 9.95%, 14.50%, 19.07%, 17.20%, 8.04%, and 7.59% (as shown in Fig. 4a), which were rates comparable to those of the PLGA microparticles ranging from about 3–13% [32,33].

In addition, the VA loading quantity was closely correlated with the dosage of the cross-linking agent (Fig. 4a). Thus, it was believed that the loading of VA was possibly related to the polymerization degree of the MIPs that was dependent upon the dosage of the cross-linking agent. As the dosage increased, the polymerization level increased, resulting in better capsulation. However, a higher polymerization degree could increase the larger size of the MIPs, inducing the rupture of some MIPs

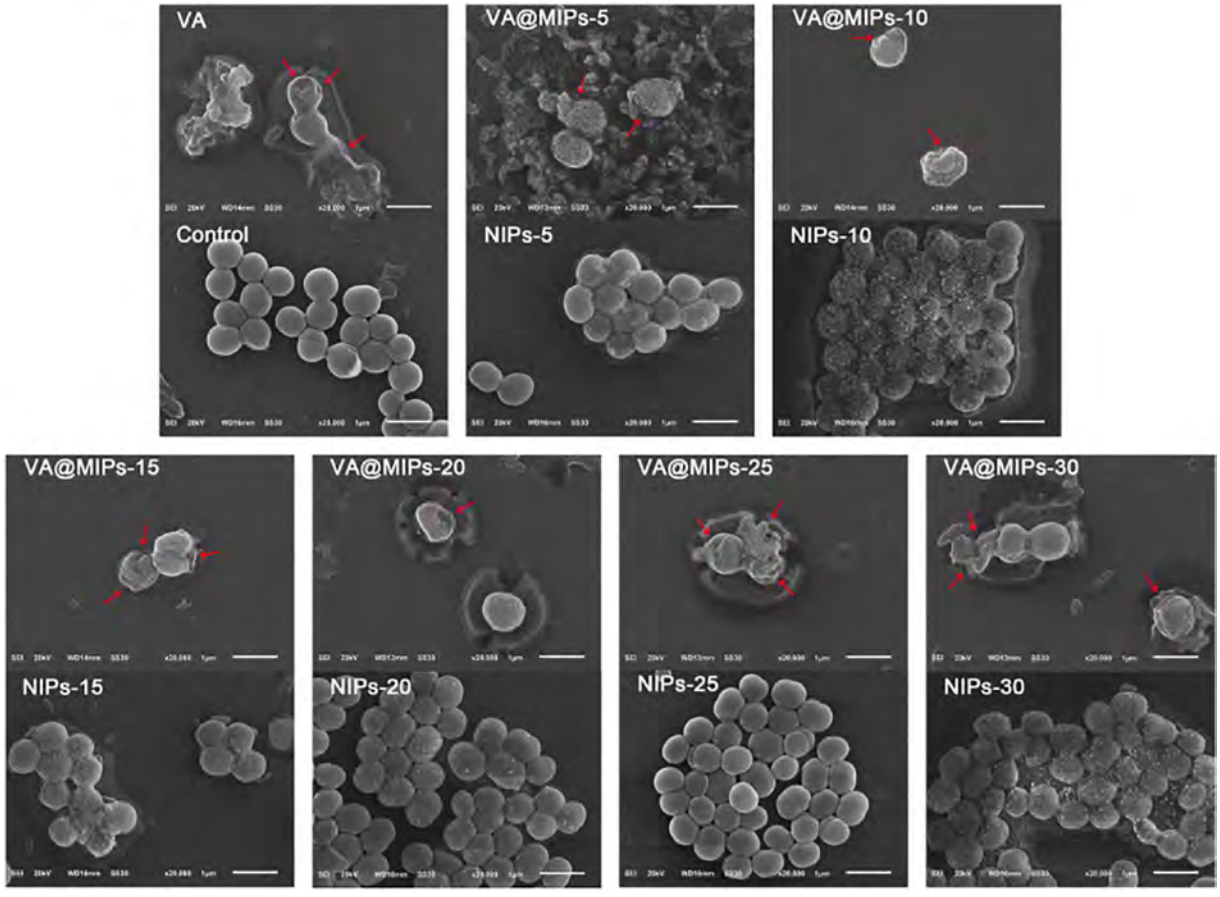

Fig. 9. SEM images of *S. aureus* after co-cultured with VA@MIPs and NIPs prepared with different dosage of EGDMA for 24 h at 37 °C.

(marked by the red arrows shown in Fig. 1) and resulting in the loss of some VA from these MIPs. This was why the MIPs-20 with the largest size had lower VA loading content than the MIPs-15. A further increase in the dosage of the cross-linking agent led to excessive cross-linking, resulting in the incomplete capsulation of the VA templates, thus inducing the decrease in the VA loading content. It should be noted that the VA loading contents of the MIPs were much higher than those of about 5% of the NIPs (shown in Fig. 4b) because the VA drug molecules were able interact with the MIPs through stronger hydrogen bonding and the adsorption caused by the nano-size effect during the loading process, while the NIPs loaded VA only by physical adsorption [34,35].

3.4. VA release

The VA release profiles of the VA@NIPs and VA@MIPs are presented in Fig. 5a and Fig. 5b, respectively. It was observed that VA was completely released from all NIPs within two days (Fig. 5a), whereas the release of VA from the MIPs extended in some cases to over 18 days, especially for VA@MIPs-20 (Fig. 5b). The different release behaviors were determined by the differences in the drug-loading mechanisms between NIPs and MIPs. The former was carried out through the weak physical adsorption between the VA molecules and the NIPs, while the latter was performed via the stronger hydrogen bonding between the VA molecules and the MIPs as well as the following capsulation. Thus, the VA release rate from the MIPs was significantly slower than that of the NIPs. Obviously, the latter could be beneficial for the long-term release of drugs. Among all of the MIP groups, VA@MIPs-20 exhibited the slowest release rate (Fig. 5b) because this group had the largest particle size of about 650 nm.

3.5. VA release behavior of the VA@MIPs-20 at different pH values

The cumulative VA release concentrations against the releasing times were plotted for different pH values for the VA@MIPs-20 group (shown in Fig. 6). In a neutral environment, the slowest release rate was exhibited, while the corresponding release rate increased significantly as the pH value decreased. For example, there was a burst-release of VA from VA@MIPs-20 at pH values of 5.2 and 6.4, as shown in the inset of Fig. 6. The former reached a stable concentration of 32 μg/mL after immersion for about 220 h, whereas it took 290 h to reach a balance of 28 μg/mL for the latter. In comparison, after immersion for 432 h in a neutral environment, the released concentration of VA from VA@MIPs-20 was about 22 μg/mL. This pH-responsive release behavior likely arose from the destruction of the hydrogen bonds between the —OH and —C—N groups as well as the —NH ($—NH_2$) and —C═O groups due to the protonation of the —C—N and —NH ($—NH_2$) groups in acidic environments. The VA loading and releasing experiments clearly confirmed that the MIPs had not only a higher VA loading capacity, but also longer-term pH-responsive VA release behavior. However, as the aforementioned in Fig. 5a, VA was completely released from all NIPs within two days in a neutral environment, indicating that VA was loaded through only a weak physical adsorption between the VA molecules and the NIPs. Hence, unlike MIPs, NIPs were not sensitive to pH. Consequently, the VA release behaviors of VA@NIPs at different pH values should be almost the same as the one at neutral PBS.

3.6. Evaluation of antibacterial activity

As shown in Fig. 7, all groups of VA@MIPs showed the matched antibacterial ratio compared to pure VA. The antibacterial ratios of pure VA, VA@MIPs-5, VA@MIPs-10, VA@MIPs-15, VA@MIPs-20, VA@MIPs-25, and VA@MIPs-30 were about 97.3%, 92.5%, 94.8%, 96.5%, 96.6%, 96.7% and 96.9%, respectively. While all of the NIPs displayed the negative antibacterial ratios compared to the control group shown in Fig. S3, indicating that the NIPs were friendly to *S. aureus*. These results are in good agreement with the observation of bacterial colonies density. As shown in Fig. 8, there are almost no viable colonies remained on the agar plate for all of the VA@MIPs and pure VA, indicating that the *S. aureus* cells had been killed. By contrast, many *S. aureus* colonies were still formed for all groups of NIPs. In addition, it exhibited much higher *S. aureus* colonies density for NIPs than those measured from the control group.

The morphologies and membrane integrity of *S. aureus* cells on the bottom of the 48-well plate were examined by SEM. Fig. 9 shows the morphologies of adherent *S. aureus*. It can be observed that there are only smaller amount of bacteria adhered on the surface of plates for all VA@MIPs and pure VA compared to NIPs and the control groups, indicating that the VA@MIPs and pure VA could restrain the growth of bacteria which is a crucial step to prevent bacterial infection [36]. Furthermore, the typical lesions and holes can be observed in *S. aureus* marked by the red arrows for the VA@MIPs and pure VA, while *S. aureus* show normal shape with spherical and smooth surface for NIPs and the control group. In addition, there are a large number of NIPs adhered on the surface of *S. aureus*, indicating that individual NIPs were friendly to *S. aureus*. Furthermore, after immersion in PBS for 2 days, the loaded VA drugs were almost completely released from all NIPs, and few residual drugs can kill *S. aureus* to some extent. So it can be concluded that NIPs could show antibacterial activities only after loading VA drugs.

4. Conclusions

The pH-sensitive VA-imprinted nanospheres were successfully prepared with the UV-initiated precipitation polymerization method. The VA loading tests showed that the MIPs had a VA loading capacity of about 17%, which was much higher than that of the NIPs. In addition, these MIPs not only exhibited a slower release rate than the NIPs, but also a long-term release duration of over 18 days. Furthermore, the synthesized VA@MIPs showed a clear response to pH values, i.e., a faster release rate and much higher release concentrations in acidic conditions than in neutral conditions, which is desirable for suppressing bacterial infections. Moreover, VA@MIPs showed much higher antibacterial ratio for more than 90% to *S. aureus*. Our results demonstrated that this drug delivery system composed of the MIPs is promising in its ability to achieve multiple biofunctions if applied as a coating on the surface of implant materials.

Acknowledgments

This work is jointly supported by the National Natural Science Foundation of China, Nos. 51422102, and 81271715, and the National Key Research and Development Program of China No. 2016YFC1100600 (sub-project 2016YFC1100604), Shenzhen Peacock Program (1108110035863317), as well as the Shenzhen Knowledge Innovation Program of Basic Research Items of Guangdong Province (Grant No.JCYJ20140414090541811), China.

Appendix A. Supplementary data

Supplementary data to this article can be found online at http://dx.doi.org/10.1016/j.msec.2017.03.259.

References

[1] P. Li, Y.F. Poon, W.F. Li, H.Y. Zhu, S.H. Yeap, Y. Cao, X.B. Qi, C.C. Zhou, M. Lamrani, R.W. Beuerman, E.T. Kang, Y.G. Mu, C.M. Li, M.W. Chang, S.S.J. Leong, M.B. Chan-Park, A polycationic antimicrobial and biocompatible hydrogel with microbe membrane suctioning ability, Nat. Mater. 10 (2011) 149–156.
[2] B.S. Necula, L.E. Fratila-Apachitei, S.A. Zaat, I. Apachitei, J. Duszczyk, In vitro antibacterial activity of porous TiO2-Ag composite layers against methicillin-resistant *Staphylococcus aureus*, Acta Biomater. 5 (2009) 3573–3580.
[3] Q. Chen, W. Li, O.M. Goudouri, Y. Ding, S. Cabanas-Polo, A.R. Boccaccini, Electrophoretic deposition of antibiotic loaded PHBV microsphere-alginate composite coating with controlled delivery potential, Colloids Surf. B 130 (2015) 199–206.

[4] M. Li, X. Liu, Z. Xu, K.W. Yeung, S. Wu, Dopamine modified organic-inorganic hybrid coating for antimicrobial and osteogenesis, ACS Appl. Mater. Interfaces 8 (2016) 33972–33981.
[5] Z. Xu, M. Li, X. Li, X. Liu, F. Ma, S. Wu, K.W.K. Yeung, Y. Han, P.K. Chu, Antibacterial activity of silver doped titanate nanowires on Ti implants, ACS Appl. Mater. Interfaces 8 (2016) 16584–16594.
[6] S.D. Pan, H.Y. Shen, L.X. Zhou, X.H. Chen, Y.G. Zhao, M.Q. Cai, M.C. Jin, Controlled synthesis of pentachlorophenol-imprinted polymers on the surface of magnetic graphene oxide for highly selective adsorption, J. Mater. Chem. A 2 (2014) 15345–15356.
[7] Y. Kanekiyo, R. Naganawa, H. Tao, pH-responsive molecularly imprinted polymers, Angew. Chem. Int. Ed. 42 (2003) 3014–3016.
[8] C. Li, Y. Ma, H. Niu, H. Zhang, Hydrophilic hollow molecularly imprinted polymer microparticles with photo- and thermoresponsive template binding and release properties in aqueous media, ACS Appl. Mater. Interfaces 7 (2015) 27340–27350.
[9] N. Li, L. Qi, Y. Shen, J. Qiao, Y. Chen, Novel oligo(ethylene glycol)-based molecularly imprinted magnetic nanoparticles for thermally modulated capture and release of lysozyme, ACS Appl. Mater. Interfaces 6 (2014) 17289–17295.
[10] R. Ahmad, N. Griffete, A. Lamouri, N. Felidj, M.M. Chehimi, C. Mangeney, Nanocomposites of gold nanoparticles@molecularly imprinted polymers: chemistry, processing, and applications in sensors, Chem. Mater. 27 (2015) 5464–5478.
[11] Q. Yan, J.Y. Yuan, Z.N. Cai, Y. Xin, Y. Kang, Y.W. Yin, Voltage-responsive vesicles based on orthogonal assembly of two homopolymers, J. Am. Chem. Soc. 132 (2010) 9268–9270.
[12] Y. Li, M.J. Ding, S. Wang, R.Y. Wang, X.L. Wu, T.T. Wen, L.H. Yuan, P. Dai, Y.H. Lin, X.M. Zhou, Preparation of imprinted polymers at surface of magnetic nanoparticles for the selective extraction of tadalafil from medicines, ACS Appl. Mater. Interfaces 3 (2011) 3308–3315.
[13] L. Li, L. Chen, H. Zhang, Y. Yang, X. Liu, Y. Chen, Temperature and magnetism bi-responsive molecularly imprinted polymers: preparation, adsorption mechanism and properties as drug delivery system for sustained release of 5-fluorouracil, Mater. Sci. Eng. C 61 (2016) 158–168.
[14] D. Shi, Integrated multifunctional nanosystems for medical diagnosis and treatment, Adv. Funct. Mater. 19 (2009) 3356–3373.
[15] Y.P. Qin, D.Y. Li, X.W. He, W.Y. Li, Y.K. Zhang, Preparation of high-efficiency cytochrome c-imprinted polymer on the surface of magnetic carbon nanotubes by epitope approach via metal chelation and six-membered ring, ACS Appl. Mater. Interfaces 8 (2016) 10155–10163.
[16] S. Lee, S. Oh, J. Lee, Y. Malpani, Y.S. Jung, B. Kang, J.Y. Lee, K. Ozasa, T. Isoshima, S.Y. Lee, M. Hara, D. Hashizume, J.M. Kim, Stimulus-responsive azobenzene supramolecules: fibers, gels, and hollow spheres, Langmuir 29 (2013) 5869–5877.
[17] M. Panagiotopoulou, Y. Salinas, S. Beyazit, S. Kunath, L. Duma, E. Prost, A.G. Mayes, M. Resmini, B. Tse Sum Bui, K. Haupt, Molecularly imprinted polymer coated quantum dots for multiplexed cell targeting and imaging, Angew. Chem. Int. Ed. 55 (2016) 8244–8248.
[18] C. Park, J. Lim, M. Yun, C. Kim, Photoinduced release of guest molecules by supramolecular transformation of self-assembled aggregates derived from dendrons, Angew. Chem. Int. Ed. 47 (2008) 2959–2963.
[19] L. Chen, S. Xu, J. Li, Recent advances in molecular imprinting technology: current status, challenges and highlighted applications, Chem. Soc. Rev. 40 (2011) 2922–2942.
[20] P. Paik, A. Gedanken, Y. Mastai, Enantioselective separation using chiral mesoporous spherical silica prepared by templating of chiral block copolymers, ACS Appl. Mater. Interfaces 1 (2009) 1834–1842.
[21] M. Esfandyari-Manesh, M. Javanbakht, F. Atyabi, A. Mohammadi, S. Mohammadi, B. Akbari-Adergani, R. Dinarvand, Dipyridamole recognition and controlled release by uniformly sized molecularly imprinted nanospheres, Mater. Sci. Eng. C 31 (2011) 1692–1699.
[22] S. Xu, H. Lu, X. Zheng, L. Chen, Stimuli-responsive molecularly imprinted polymers: versatile functional materials, J. Mater. Chem. C 1 (2013) 4406–4422.
[23] R. Suedee, C. Jantarat, W. Lindner, H. Viernstein, S. Songkro, T. Srichana, Development of a pH-responsive drug delivery system for enantioselective-controlled delivery of racemic drugs, J. Control. Release 142 (2010) 122–131.
[24] V. Yarlagadda, P. Sarkar, S. Samaddar, J. Haldar, A vancomycin derivative with a pyrophosphate-binding group: a strategy to combat vancomycin-resistant bacteria, Angew. Chem. Int. Ed. 55 (2016) 7836–7840.
[25] Y. Bu, L. Zhang, J. Liu, L. Zhang, T. Li, H. Shen, X. Wang, F. Yang, P. Tang, D. Wu, Synthesis and properties of hemostatic and bacteria-responsive in situ hydrogels for emergency treatment in critical situations, ACS Appl. Mater. Interfaces 8 (2016) 12674–12683.
[26] C.C. Yang, C.C. Lin, J.W. Liao, S.K. Yen, Vancomycin-chitosan composite deposited on post porous hydroxyapatite coated Ti6Al4V implant for drug controlled release, Mater. Sci. Eng. C 33 (2013) 2203–2212.
[27] U. Hess, G. Mikolajczyk, L. Treccani, P. Streckbein, C. Heiss, S. Odenbach, K. Rezwan, Multi-loaded ceramic beads/matrix scaffolds obtained by combining ionotropic and freeze gelation for sustained and tuneable vancomycin release, Mater. Sci. Eng. C 67 (2016) 542–553.
[28] J. Wang, J. Li, S. Qian, G. Guo, Q. Wang, J. Tang, H. Shen, X. Liu, X. Zhang, P.K. Chu, Antibacterial surface design of titanium-based biomaterials for enhanced bacteria-killing and cell-assisting functions against periprosthetic joint infection, ACS Appl. Mater. Interfaces 8 (2016) 11162–11178.
[29] T. Zhou, Y. Zhu, X. Li, X. Liu, K.W.K. Yeung, S. Wu, X. Wang, Z. Cui, X. Yang, P.K. Chu, Surface functionalization of biomaterials by radical polymerization, Prog. Mater. Sci. 83 (2016) 191–235.
[30] M.D. Pawar, G.V. Rathna, S. Agrawal, B.S. Kuchekar, Bioactive thermoresponsive polyblend nanofiber formulations for wound healing, Mater. Sci. Eng. C 48 (2015) 126–137.
[31] C. Cacho, E. Turiel, A. Martin-Esteban, C. Perez-Conde, C. Camara, Characterisation and quality assessment of binding sites on a propazine-imprinted polymer prepared by precipitation polymerisation, J. Chromatogr. B 802 (2004) 347–353.
[32] S. Jaraswekin, S. Prakongpan, R. Bodmeier, Effect of poly(lactide-co-glycolide) molecular weight on the release of dexamethasone sodium phosphate from microparticles, J. Microencapsul. 24 (2007) 117–128.
[33] J. Mosafer, M. Teymouri, K. Abnous, M. Tafaghodi, M. Ramezani, M. Study and evaluation of nucleolin-targeted delivery of magnetic PLGA-PEG nanospheres loaded with doxorubicin to C6 glioma cells compared with low nucleolin-expressing L929 cells, Mater. Sci. Eng. C 72 (2017) 123–133.
[34] L. Jiang, L. Gao, Effect of Tiron adsorption on the colloidal stability of nano-sized alumina suspension, Mater. Chem. Phys. 80 (2003) 157–161.
[35] M.P. Ginebra, F.C. Driessens, J.A. Planell, Effect of the particle size on the micro and nanostructural features of a calcium phosphate cement: a kinetic analysis, Biomaterials 25 (2004) 3453–3462.
[36] S.B. Liu, L. Wei, L. Hao, N. Fang, M.W. Chang, R. Xu, Y.H. Yang, Y. Chen, Sharper and faster "nano darts" kill more bacteria: a study of antibacterial activity of individually dispersed pristine single-walled carbon nanotube, ACS Nano 3 (2009) 3891–3902.

Supporting Information

The controlled drug release by pH-sensitive molecularly imprinted nanospheres for enhanced antibacterial activity

*Congyang Mao [a], Xianzhou Xie [a], Xiangmei Liu [a], Zhenduo Cui [b], Xianjin Yang [b], K.W. K. Yeung[c], Haobo Pan [d], Paul K Chu [e], Shuilin Wu [a,b]**

[a] Hubei Collaborative Innovation Center for Advanced Organic Chemical Materials, Ministry-of-Education Key Laboratory for the Green Preparation and Application of Functional Materials, Hubei Key Laboratory of Polymer Materials, School of Materials Science & Engineering, Hubei University, Wuhan 430062, China

[b] School of Materials Science & Engineering, Tianjin University, Tianjin 300072, China

[c] Department of Orthopaedics & Traumatology, Li Ka Shing Faculty of Medicine, The University of Hong Kong, Pokfulam, Hong Kong, China

[d] Center for Human Tissues and Organs Degeneration, Shenzhen Institutes of Advanced Technology, Chinese Academy of Sciences, Shenzhen 518055, China

[e] Department of Physics & Materials Science, City University of Hong Kong, Tat Chee Avenue, Kowloon, Hong Kong, China

* To whom correspondence should be addressed:

E-mail: shuilin.wu@gmail.com; sxwsl1976@163.com (S.L. Wu)T

Table of contents in supporting information

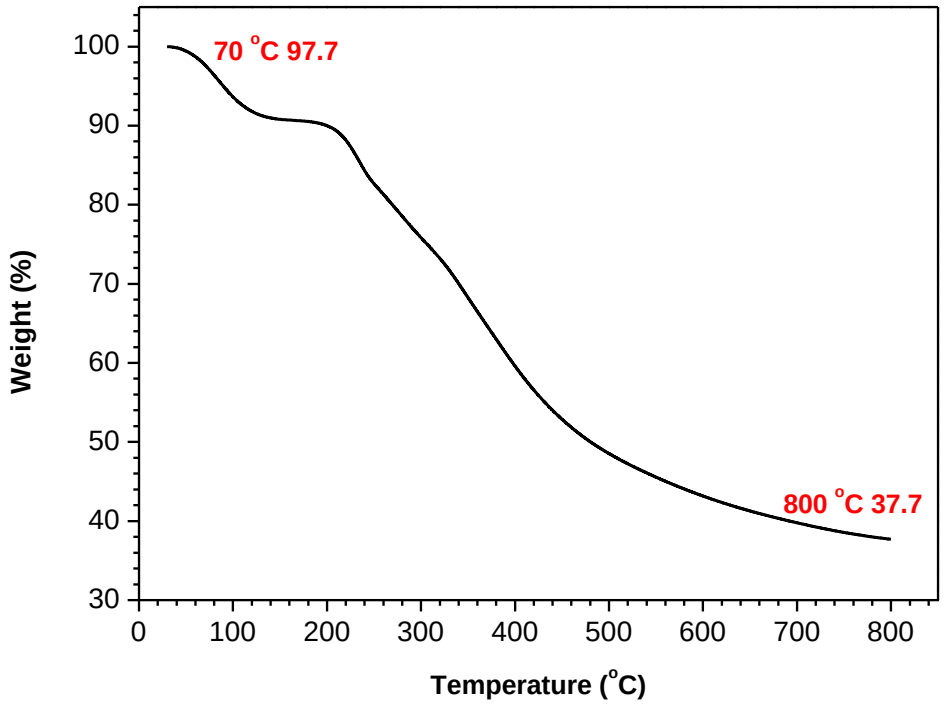

Figure S1. TGA profile of vancomycin from 30 ºC -800 ºC. The residual mass fractions of vancomycin were 97.7% and 27.7 at 70 ºC and 800 ºC, respectively.

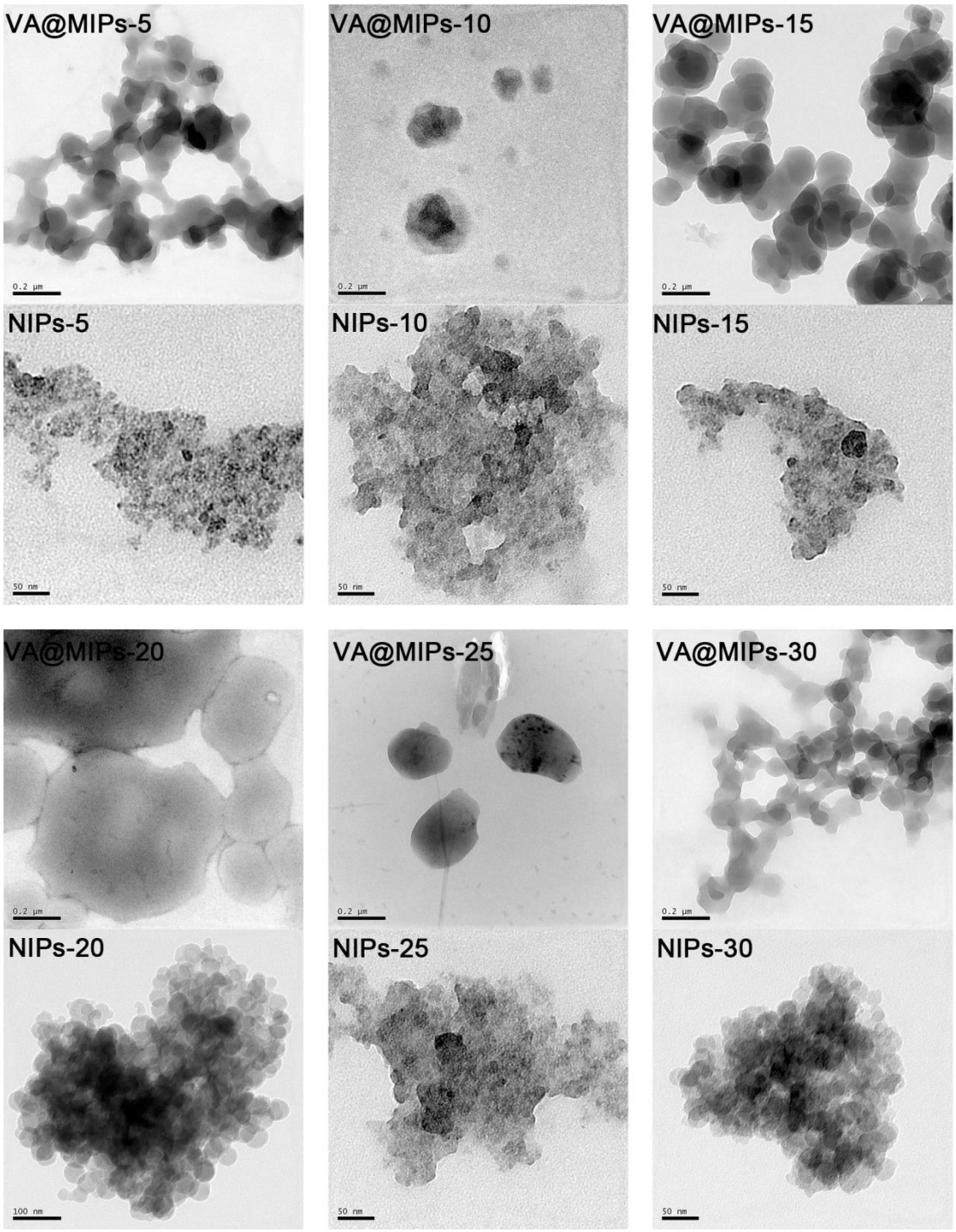

Figure S2. TEM images of the VA@MIPs and NIPs prepared with different dosage of cross-linker EGDMA.

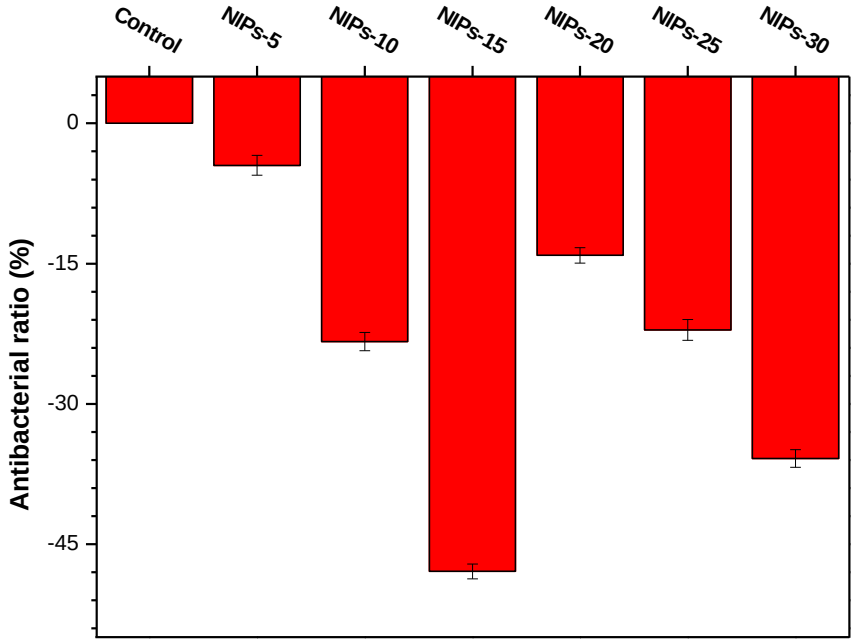

Figure S3. Antibacterial activity of the NIPs prepared with different dosage of EGDMA against *S. aureus* after 24 h incubation at 37 ºC (n=3).